

# Compact Nuclear Starbursts in Seyfert 2 Galaxies from the CfA and 12 $\mu$ m Samples

Masatoshi Imanishi<sup>1,2,3</sup>

*National Astronomical Observatory, Mitaka, 2-21-1, Osawa, Tokyo 181-8588, Japan*

imanishi@optik.mtk.nao.ac.jp

## ABSTRACT

We present infrared 2.8–4.1  $\mu$ m slit spectra of 32 Seyfert 2 galaxies in the CfA and 12  $\mu$ m samples. The 3.3  $\mu$ m polycyclic aromatic hydrocarbon (PAH) emission feature was used to estimate the absolute magnitude of a compact nuclear starburst (less than a few hundred parsecs in size) that is presumed to have occurred in the outer region of an obscuring dusty molecular torus around a central supermassive black hole. We detected 3.3  $\mu$ m PAH emission in 11 of the 32 Seyfert 2 nuclei in our sample, providing evidence for the presence of compact nuclear starbursts in a significant fraction of Seyfert 2 nuclei. However, the rest-frame equivalent widths of the 3.3  $\mu$ m PAH emission, and the 3.3  $\mu$ m PAH-to-infrared luminosity ratios measured in this study suggest that compact nuclear starbursts generally do not contribute significantly to the observed 3–4  $\mu$ m nuclear fluxes or to the infrared luminosities of Seyfert 2 galaxies. Absorption features at 3.4  $\mu$ m from bare dust were clearly detected in only two of the nuclei, and features at 3.1  $\mu$ m from ice-covered dust were detected in only one nucleus. If the dust properties in the direction of these Seyfert 2 nuclei do not differ significantly from the Galactic interstellar medium, then these small absorption optical

---

<sup>1</sup>Visiting Astronomer at the Infrared Telescope Facility, which is operated by the University of Hawaii under Cooperative Agreement no. NCC 5-538 with the National Aeronautics and Space Administration, Office of Space Science, Planetary Astronomy Program.

<sup>2</sup>Based in part on data collected at Subaru Telescope, which is operated by the National Astronomical Observatory of Japan.

<sup>3</sup>Department of Astronomy, School of Science, Graduate University for Advanced Studies, Mitaka, Tokyo 181-8588

depths suggest that dust extinction toward the 3–4  $\mu\text{m}$  continuum-emitting region in the innermost part of the obscuring dusty torus is modest:  $A_V < 50\text{--}60$  mag. Finally, the 3.3  $\mu\text{m}$  PAH emission luminosities measured in this study were found to be significantly correlated with *IRAS* 12- and 25- $\mu\text{m}$ , and nuclear *N*-band (10.6  $\mu\text{m}$ ) luminosities. If these three luminosities trace the power of the active galactic nucleus (AGN), then the luminosities of compact nuclear starbursts and AGNs are correlated. This correlation is in agreement with theories predicting that the presence of a compact nuclear starburst in the torus leads to an enhancement of the mass accretion rate onto the central supermassive black hole.

*Subject headings:* galaxies: Seyfert — galaxies: nuclei — infrared: galaxies

## 1. Introduction

Seyferts are the most numerous class of active galactic nuclei (AGNs). The two types of Seyfert galaxies, type 1 (with broad optical emission lines) and type 2 (with no such lines), can be unified by the combination of an obscuring dusty molecular torus around a central, accreting supermassive black hole, and different viewing angles (Antonucci 1993). As dusty tori are rich in molecular gas, they are natural sites for starbursts to occur (Fabian et al. 1998). For several reasons, such a *nuclear* starburst in the torus is likely to occur at the outer part, as originally proposed by Heckman et al. (1997). First, for a dusty molecular torus whose mass is significantly smaller than the central supermassive black hole (Taniguchi & Murayama 1998), gas in the torus rotates in a Keplerian manner, and the gravitational stability parameter  $Q$  (Toomre 1964) is described as  $Q = \sigma\Omega/\pi G\Sigma_{\text{gas}}$ , where  $\sigma$ ,  $\Omega$ , and  $\Sigma_{\text{gas}}$  are the gas velocity dispersion, angular velocity, and gas surface density, respectively. In the case of a power-law radial density distribution of gas ( $\Sigma_{\text{gas}} \propto r^{-\alpha}$ ; where  $r$  is the distance from the central supermassive black hole) in an isothermal Keplerian disk ( $\Omega \propto r^{-1.5}$ ),  $Q$  is proportional to  $r^{\alpha-1.5}$ . If the radial density distribution of gas and dust in the torus is flatter than  $r^{-1.5}$ , as is often assumed (Barvainis 1987; Granato & Danese 1994; Rowan-Robinson 1995; Efstathiou & Rowan-Robinson 1995), then  $Q$  decreases with radius, so that the gravitational collapse of molecular gas can occur more easily in the outer regions of the torus (Wada & Norman 2002). In addition, star formation in the inner part of the torus could be suppressed due to strong X-ray radiation from the AGN (Cid Fernandes & Terlevich 1995). Finally, if there is molecular gas inflow from the host galaxy to the torus, gas compression will occur at the outer edges of the torus, encouraging star formation.

Such compact nuclear starbursts have been detected in some Seyfert nuclei (Gonzalez

Delgado et al. 1998; Oliva et al. 1999; Storchi-Bergmann et al. 2000; Gonzalez Delgado et al. 2001; Cid Fernandes et al. 2001; Kohno et al. 2002). However, their absolute luminosities and relation to the central AGNs are still unclear. Infrared 2.8–4.1  $\mu\text{m}$  spectroscopy is one of the most powerful ways of detecting and quantitatively estimating the energetic importance of these compact nuclear starbursts (Imanishi 2002; Rodriguez-Ardila & Viegas 2003). First, starburst emission is clearly distinguishable from emission from the AGN, using the polycyclic aromatic hydrocarbon (PAH) emission found at 3.3  $\mu\text{m}$ . In a *normal* starburst, PAHs widely distributed in the interstellar medium are excited by far-UV photons from stars, and so strong 3.3  $\mu\text{m}$  PAH emission is usually detected (Moorwood 1986). Close to an AGN, where sufficient far-UV photons from the AGN are available, X-ray radiation is also strong, which destroys PAHs (Voit 1992). At a certain distance from the central AGN in the obscuring material, the X-ray flux is sufficiently attenuated to prevent this. However, as UV photons have a higher susceptibility to extinction than X-rays, far-UV photons from the AGN are not expected to survive to these distances. Thus, no PAH emission is expected in a *pure* AGN. The detection of 3.3  $\mu\text{m}$  PAH emission from an AGN requires far-UV photons from a starburst to be sufficiently shielded from AGN emission, as is the case for a compact nuclear starburst occurring in the outer part of a dusty torus. The PAH emission luminosity is therefore expected to roughly trace the magnitude of such a starburst. Another advantage of infrared 2.8–4.1  $\mu\text{m}$  spectroscopy is that the flux attenuation is lower, as dust extinction at 2.8–4.1  $\mu\text{m}$  is much less than at UV or optical wavelengths. The absolute magnitude of a starburst in a Seyfert can be determined from the *observed* 3.3  $\mu\text{m}$  PAH emission luminosity (Imanishi 2002). Finally, since 3.3  $\mu\text{m}$  PAH emission is intrinsically strong (Imanishi & Dudley 2000), even the signature of a weak starburst is detectable with a spectrum of typical signal-to-noise ratio. Using infrared 2.8–4.1  $\mu\text{m}$  slit spectroscopy, it has been possible to detect and quantify previously undetected compact nuclear starbursts in Seyferts (Imanishi 2002; Rodriguez-Ardila & Viegas 2003).

The physical scale of a compact nuclear starburst in the outer region of a dusty molecular torus is less than a few hundred parsecs, which corresponds to less than 1–2 arcsec in the majority of Seyferts at  $z > 0.007$ . In Seyferts, extended *circumnuclear* ring-shaped starbursts are found typically at distances of  $\sim 1$  kpc from the nuclei (Storchi-Bergmann, Wilson, & Baldwin 1996; Storchi-Bergmann et al. 1996), and are generally more powerful than the compact *nuclear* starbursts (Le Floc’h et al. 2001; Imanishi 2002). Hence, the use of a narrow ( $< 1$ –2 arcsec) slit is most effective to distinguish between extended starbursts and the compact nuclear starbursts that are of interest. Therefore, we have performed ground-based infrared 2.8–4.1  $\mu\text{m}$  slit spectroscopy focusing initially on Seyfert 2 nuclei to determine observational constraints on the properties of compact nuclear starbursts. Throughout this paper,  $H_0 = 75 \text{ km s}^{-1} \text{ Mpc}^{-1}$ ,  $\Omega_M = 0.3$ , and  $\Omega_\Lambda = 0.7$  are adopted.

## 2. Targets

Seyfert 2 galaxies in the CfA (Huchra & Burg 1992) and  $12\mu\text{m}$  (Rush, Malkan, & Spinoglio 1993) samples were selected based on their host galaxy magnitudes and *IRAS*  $12\mu\text{m}$  fluxes, respectively. These samples are not expected to be biased toward or against the presence of compact nuclear starbursts, and is thus suitable for our program. The following sample selection criteria were employed: (1) In very nearby sources, slit spectroscopy may miss a significant fraction of emission from compact nuclear starbursts with a physical size scale of up to a few hundred pc. The slit width used,  $0''.9-1''.6$  (§3), corresponds to 120–220 pc at  $z = 0.007$ . Seyfert 2s at  $z < 0.007$  are thus excluded. (2) In distant Seyfert 2s, slit spectroscopy may be significantly contaminated by extended (kpc scale) powerful circumnuclear starbursts. The slit width used corresponds to 600 pc – 1 kpc at  $z = 0.035$ . Seyfert 2s at  $z > 0.035$  are excluded. (3)  $12\mu\text{m}$  Seyfert 2s at declination  $< -35^\circ$  are excluded because they are not observable under good observing conditions from Mauna Kea, Hawaii. (4) Some  $12\mu\text{m}$  Seyfert 2s in Rush et al. (1993) have been later re-classified as LINERs or HII-region galaxies based on higher quality optical spectra (Tran 2003). These sources are excluded. All CfA Seyfert 2s later re-observed by Osterbrock & Martel (1993) were re-classified as Seyfert 1.8, 1.9, or 2. These sources are included.

These selection criteria result in 18 CfA Seyfert 2s and 26  $12\mu\text{m}$  Seyfert 2s, of which six sources are included in both samples. From the total sample of 38 Seyfert 2s, 32 (32/38 = 84%) sources have been observed so far. Table 1 summarizes the infrared emission properties of the 32 observed Seyfert 2s. The six unobserved sources are UGC 1395 (=0152+06), NGC 3362, UGC 6100 (=A1058+45), UGC 8621 (=1335+39), and NGC 5283 in the CfA sample, and MCG-2-8-39 in the  $12\mu\text{m}$  sample. Although the sample is not statistically complete, major conclusions drawn from the 32 sources in this paper are unlikely to be affected significantly by omission of the six unobserved sources.

## 3. Observations and Data Analysis

The observing log is shown in Table 2. Observations were made with the UKIRT CGS4 (Mountain et al. 1990), the IRTF NSFCAM (Shure et al. 1994), the IRTF SpeX (Rayner et al. 2003), and the Subaru IRCS (Kobayashi et al. 2000), on Mauna Kea, Hawaii. Details of the observations with the UKIRT CGS4 (for NGC 7172) and the IRTF NSFCAM (for NGC 5256 and NGC 5135) were described by Imanishi (2000) and Imanishi (2002), respectively, and are not repeated here.

For the IRTF SpeX observing run, the 1.9–4.2  $\mu\text{m}$  cross-dispersed mode with a  $1''.6$

wide slit was employed. The achievable spectral resolution at  $3.5 \mu\text{m}$  is  $R \sim 450$ . The sky conditions were photometric and the seeing sizes at  $K$  ( $2.2 \mu\text{m}$ ) were  $0''.6$ – $0''.9$  (full-width at half-maximum; FWHM) throughout the observations. The position angle of the slit was set along the north-south direction. A standard telescope nodding technique (ABBA pattern) with a throw of  $7.5$  arcsec was employed along the slit to subtract background emission. As  $3$ – $4 \mu\text{m}$  emission from a Seyfert 2 galaxy is usually dominated by compact nuclear emission (Alonso-Herrero et al. 1998), this throw is believed to be sufficiently large. The telescope tracking was monitored with the infrared slit-viewer of SpeX. Each exposure was  $15$  sec, and  $2$  coadds were made at each position. With this exposure time, signals at  $\lambda_{\text{obs}} > 4.1 \mu\text{m}$  (in the observed frame) exceed the linearity level of the SpeX array, and so data at  $\lambda_{\text{obs}} > 4.1 \mu\text{m}$  were removed.

For the Subaru IRCS observing run, a  $0''.9$ -wide slit and the  $L$ -grism were used with a  $58$ -mas pixel scale. The achievable spectral resolution at  $3.5 \mu\text{m}$  is  $R \sim 140$ . The sky was not completely photometric during the observations of some of the Seyfert 2 nuclei (Mrk 334, NGC 1144, and NGC 1125). The position angle of the slit was set along the east-west direction, except in the case of NGC 1144 where the angle was set along the north-south direction. The seeing at  $K$  was  $0''.5$ – $0''.8$  in FWHM. A standard telescope nodding technique (ABBA pattern), with a throw of  $7$  arcsec along the slit, was employed. Each exposure was  $2.0$ – $3.0$  sec, and  $15$ – $30$  coadds were made at each slit position. Data at  $\lambda_{\text{obs}} > 4.1 \mu\text{m}$  were removed, due to signal levels above the linearity level of the IRCS array.

A-, F-, and G-type standard stars (Table 2) were observed with airmass difference of  $< 0.1$  to the individual Seyfert 2 nuclei, to correct for the transmission of the Earth’s atmosphere. The  $L$ -band ( $3.5 \mu\text{m}$ ) magnitudes of standard stars were estimated from their  $V$ -band ( $0.6 \mu\text{m}$ ) magnitudes, adopting the  $V - L$  colors appropriate to the stellar types of individual standard stars (Tokunaga 2000).

Standard data analysis procedures were employed using IRAF <sup>4</sup>. Initially, bad pixels and pixels hit by cosmic rays were replaced with the interpolated values of the surrounding pixels. Then, frames taken with an A (or B) beam were subtracted from frames subsequently taken with a B (or A) beam, and the resulting subtracted frames were added and were divided by a spectroscopic flat image. The Seyfert 2 and standard star spectra were then extracted by integrating signals over  $2''.4$ – $3''.0$  and  $1''.4$ – $1''.8$  along the slit for the IRTF SpeX and Subaru IRCS data, respectively. Wavelength calibration was performed using the

---

<sup>4</sup>IRAF is distributed by the National Optical Astronomy Observatories, which are operated by the Association of Universities for Research in Astronomy, Inc. (AURA), under cooperative agreement with the National Science Foundation.

wavelength-dependent transmission of the Earth’s atmosphere. The Seyfert 2 spectra were divided by those of the corresponding standard stars, and were multiplied by the spectra of blackbodies with temperatures corresponding to those of the individual standard stars (Table 2).

All of the IRTF SpeX observing runs and Subaru IRCS runs in 2003 March were made under photometric sky conditions, and so flux calibration was made based on the signal detected inside our slit. For the CfA sample Seyfert 2s, *L*-band (3.5  $\mu\text{m}$ ) photometry taken with 1''5–8''6 apertures was available (Ivanov et al. 2000; Alonso-Herrero et al. 2003). Our flux calibration generally agrees with or is slightly ( $<1$  mag) fainter than their photometry, which is reasonable because 3–4  $\mu\text{m}$  continuum emission from a Seyfert 2 galaxy is usually dominated by compact nuclear emission, but emission more extended than our slit size also exists (Alonso-Herrero et al. 1998, 2001, 2003). During the observations of Mrk 334, NGC 1125, and NGC 1144, the sky was not completely photometric due to the presence of thin cirrus. For Mrk 334 and NGC 1144, *L*-band photometry made with a 1.5 arcsec aperture by Alonso-Herrero et al. (2003) was used for the flux calibration of our slit spectra. For NGC 1125, although no *L*-band photometry was available, the cirrus was thinner than during the observations of Mrk 334 and NGC 1144, and the flux discrepancy among independent data sets is small ( $<20\%$ ). The flux was thus calibrated using our slit spectra.

Appropriate spectral binning was applied for faint sources, particularly at  $\lambda_{\text{obs}} < 3.3$   $\mu\text{m}$ . In this wavelength range, the Earth’s atmospheric transmission is highly wavelength dependent, and even displacement at the sub-pixel level between a Seyfert 2 and corresponding standard star along the wavelength direction could produce a spiky spectrum. Binning to a spectral resolution of  $R < 100$  can help reduce these spurious spikes (Imanishi & Maloney 2003). The targeted feature in this wavelength range is the 3.1  $\mu\text{m}$  absorption feature caused by ice-covered dust grains, which is sufficiently broad (Smith, Sellgren, & Tokunaga 1989) that a spectral resolution of  $R > 50$  allows investigation of its properties. In the vicinity of the redshifted 3.3  $\mu\text{m}$  PAH emission feature ( $\lambda_{\text{rest}} \sim 3.29$   $\mu\text{m}$ ), a spectral resolution of  $R > 100$  was retained to properly trace its profile and estimate its flux reliably. For faint sources, data at the longer side of 3.3  $\mu\text{m}$  PAH emission were also binned. The main targeted feature in this wavelength range is the absorption feature due to bare carbonaceous dust at  $\lambda_{\text{rest}} \sim 3.4$   $\mu\text{m}$  (Imanishi & Dudley 2000; Imanishi et al. 2001). As this feature is broad and weak, a spectral resolution of  $R > 100$  is sufficient.

#### 4. Results

Figure 1 shows flux-calibrated 2.8–4.1  $\mu\text{m}$  slit spectra. For NGC 5256 and NGC 5135, the 3.0–4.0  $\mu\text{m}$  spectra were presented by Imanishi (2002). Here, 2.8–4.1  $\mu\text{m}$  spectra are shown, which illustrate the properties of the broad 3.1  $\mu\text{m}$  absorption feature. The spectrum of NGC 7172 was taken with UKIRT CGS4, so the wavelength coverage is  $\lambda_{\text{obs}} = 3.2\text{--}3.8$   $\mu\text{m}$ . The spectrum presented by Imanishi (2000) is shown again here.

In the 2.8–4.1  $\mu\text{m}$  spectra shown in Figure 1, we consider 3.3  $\mu\text{m}$  PAH emission to be detected when at least two successive data points are significantly higher than the continuum level. Using this criterion, 3.3  $\mu\text{m}$  PAH emission was detected in 11 of the 32 observed Seyfert 2 nuclei. The detection rates are 31% (4/13) and 36% (9/25) for CfA and 12  $\mu\text{m}$  Seyfert 2s, respectively. The fluxes, luminosities, and rest-frame equivalent widths of the 3.3  $\mu\text{m}$  PAH emission were estimated using the method described by Imanishi (2002) and are summarized in Table 3.

If sufficiently obscured AGN emission contributes significantly to an observed 3–4  $\mu\text{m}$  nuclear flux, the 3.4  $\mu\text{m}$  absorption feature due to bare carbonaceous dust grains (Imanishi & Dudley 2000; Imanishi et al. 2001) and/or the 3.1  $\mu\text{m}$  absorption feature due to ice-covered dust grains (Imanishi & Maloney 2003) should be detected. The 3.4  $\mu\text{m}$  absorption feature was clearly detected in only F04385–0828 and NGC 7172, with an optical depth of  $\sim 0.1$ . The presence of the 3.1  $\mu\text{m}$  absorption feature was inferred only in NGC 4388.

In some bright nearby sources (NGC 4388, NGC 262, NGC 1194, NGC 4968 MCG-3-34-64, and MCG-2-40-4) for which sufficient signal-to-noise ratios in the continuum are achieved even without spectral binning, [SiIV] emission at  $\lambda_{\text{rest}} = 3.94$   $\mu\text{m}$  and Br $\alpha$  emission at  $\lambda_{\text{rest}} = 4.05$   $\mu\text{m}$  are detected. These emission lines are sufficiently strong in NGC 4388 and NGC 4968 that reliable flux estimates for these relatively narrow emission lines (narrower than PAH) are possible even in our low-resolution spectra. For NGC 4388, the observed [SiIX] and Br $\alpha$  emission fluxes are estimated to be  $3 \times 10^{-17}$  W m $^{-2}$  and  $4 \times 10^{-17}$  W m $^{-2}$ , respectively. For NGC 4968, they are  $1 \times 10^{-17}$  W m $^{-2}$  and  $2 \times 10^{-17}$  W m $^{-2}$ , respectively. These fluxes are slightly higher than the estimates by Lutz et al. (2002), possibly due to our larger slit size.

## 5. Discussion

### 5.1. Compact Nuclear Starbursts

To investigate the contribution from compact nuclear starbursts to the observed 3–4  $\mu\text{m}$  fluxes and to the total infrared (8–1000  $\mu\text{m}$ ) luminosities, the rest-frame equivalent widths of 3.3  $\mu\text{m}$  PAH emission features ( $\text{EW}_{3.3\text{PAH}}$ ) and 3.3  $\mu\text{m}$  PAH-to-infrared luminosity ratios ( $L_{3.3\text{PAH}}/L_{\text{IR}}$ ) are shown in Table 3, as described in Imanishi (2002).

As an equivalent width ( $\equiv$  the ratio of line to continuum flux) is, by definition, robust to dust extinction, a large PAH equivalent width ( $\sim 100$  nm; Imanishi & Dudley 2000) should always be detected in a starburst galaxy, regardless of dust extinction. All but NGC 5256 and Mrk 938 show  $\text{EW}_{3.3\text{PAH}}$  more than a factor of two smaller than  $\sim 100$  nm. Therefore, although the compact nuclear starbursts are detected at 3–4  $\mu\text{m}$  in  $\sim 30\%$  (11/32) of Seyfert 2s, their observed 3–4  $\mu\text{m}$  fluxes, except NGC 5256 and Mrk 938, should be dominated by a continuum that does not show a strong 3.3  $\mu\text{m}$  PAH emission feature. AGN-powered hot ( $\sim 800$ – $1000$  K) dust in the very inner part of an obscuring dusty torus (Barvainis 1987) close to the innermost dust sublimation radius (which corresponds to 1000–1800 K dust; Granato et al. 1997) can emit 3–4  $\mu\text{m}$  continuum efficiently (assuming a blackbody spectrum), without strong 3.3  $\mu\text{m}$  PAH emission. Thus, it can be concluded that the 3–4  $\mu\text{m}$  fluxes in the majority of the observed Seyfert 2 nuclei originate in featureless continuum emission from hot dust powered by an AGN.

The  $L_{3.3\text{PAH}}/L_{\text{IR}}$  ratios in all Seyfert 2s (Table 3) are a factor of  $\gtrsim 2$  smaller than the ratios for starburst-dominated galaxies ( $\sim 1 \times 10^{-3}$ ; Mouri et al. 1990; Imanishi 2002). Thus, compact nuclear starbursts are unlikely to dominate the infrared luminosities of these Seyfert 2 galaxies. The larger sample presented here confirms the small  $\text{EW}_{3.3\text{PAH}}$  and  $L_{3.3\text{PAH}}/L_{\text{IR}}$  found previously in a smaller sample of Seyfert 2s (Imanishi 2002).

### 5.2. Dust Extinction toward the Innermost 3–4 $\mu\text{m}$ Continuum-emitting Regions in Seyfert 2 Nuclei

As it has been shown in §5.1 that the observed 3–4  $\mu\text{m}$  fluxes in the majority of the observed Seyfert 2 nuclei are dominated by AGN-powered hot-dust emission in the innermost part of the obscuring dusty torus, the observed optical depths of the absorption features at 3.4  $\mu\text{m}$  and 3.1  $\mu\text{m}$  reflect the column density of obscuring dust toward the innermost 3–4  $\mu\text{m}$  continuum-emitting regions. In the Galaxy, dust grains located deep inside molecular gas are covered with an ice mantle, if they are sufficiently shielded from ambient UV radiation

(Whittet et al. 1988). Such dust grains show an absorption feature at  $3.1 \mu\text{m}$  (Smith et al. 1989), but no significant feature at  $3.4 \mu\text{m}$  (Mennella et al. 2001). Dust absorption at  $3.4 \mu\text{m}$  is detected in the diffuse interstellar medium (Pendleton et al. 1994; Imanishi et al. 1996; Rawlings, Adamson, & Whittet 2003) where dust grains are not covered with an ice mantle (that is, “bare”). As dust extinction toward the innermost  $3\text{--}4 \mu\text{m}$  continuum-emitting hot dust around an AGN can be fitted with a foreground-screen dust model, the total column density of obscuring dust, including both bare and ice-covered dust grains, can be estimated in a fairly straightforward manner from the optical depths of these absorption features ( $\tau_{3.1}$  and  $\tau_{3.4}$ ).

The  $\tau_{3.4}$  values for the two detected sources (F04385–0828 and NGC 7172) are  $\sim 0.1$ . Conservative upper limits for  $\tau_{3.4}$  in the remaining undetected sources are  $< 0.2$ . The  $\tau_{3.1}$  value for NGC 4388 is  $\sim 0.2$ , some fraction of which may originate in dust in the edge-on host galaxy (Pogge & Martini 2002), rather than the dusty torus. Conservative upper limits for  $\tau_{3.1}$  for the remaining sources are  $< 0.3$ . If the obscuring dust toward these Seyfert 2 nuclei shows a dust extinction curve similar to that of the Galaxy ( $\tau_{3.4}/A_V = 0.004\text{--}0.007$ ; Pendleton et al. 1994,  $\tau_{3.1}/A_V \sim 0.06$ ; Smith, Sellgren, & Brooke 1993; Tanaka et al. 1990; Murakawa, Tamura, & Nagata 2000), then the  $\tau_{3.1}$  and  $\tau_{3.4}$  values imply that  $A_V < 50$  mag and  $< 5$  mag for bare and ice-covered dust grains, respectively. Hence, the total dust column density toward the innermost  $3\text{--}4 \mu\text{m}$  continuum-emitting hot dust around a central AGN is modest,  $A_V < 50\text{--}60$  mag, in the majority of Seyfert 2 nuclei.

If the  $\tau_{3.4}/A_V$  ratios toward these Seyfert 2 nuclei are substantially smaller than the Galactic ratio, then the  $A_V$  value estimated in this way is underestimated in Seyfert 2s. In the dusty torus around an AGN, the dust size may be larger than in the Galactic interstellar medium, due to dust coagulation (Maiolino et al. 2001a,b; Imanishi 2001), and the  $9.7 \mu\text{m}$  silicate dust feature may be weakened (Laor & Draine 1993). It is possible that the  $3.4 \mu\text{m}$  absorption feature is also weakened and the  $\tau_{3.4}/A_V$  ratio toward an obscured AGN is smaller than the Galactic value. However, in a number of obscured AGNs, it has been found that the dereddened AGN luminosity based on the Galactic  $\tau_{3.4}/A_V$  ratio is comparable to the bolometric luminosity (Imanishi et al. 2001; Imanishi & Maloney 2003). If  $\tau_{3.4}/A_V$  ratios in these obscured AGNs are substantially smaller than the Galactic ratio, then the dereddened AGN luminosities would substantially exceed the bolometric luminosities. It is thus unlikely that the  $\tau_{3.4}/A_V$  ratio toward an obscured AGN is substantially smaller than the Galactic value, so that our estimate for dust extinction in these Seyfert 2s appears reasonable. Indeed, the estimated modest dust extinction toward the majority of Seyfert 2 nuclei, excluding the dustiest, most infrared-luminous examples (ultraluminous infrared galaxies), is generally in good agreement with other independent estimates. First, infrared spectral energy distributions of Seyferts show similarly modest dust extinction (Granato,

Danese, & Franceschini 1997; Dopita et al. 1998; Fadda et al. 1998). In addition, Alonso-Herrero, Ward, & Kotilainen (1997) found that dust extinction toward the innermost  $3.5 \mu\text{m}$  continuum-emitting regions is  $A_V < 50\text{--}60$  mag, based on a comparison of the luminosities of optical [OIII] emission lines from unobscured regions and  $3.5 \mu\text{m}$  continuum. Finally, Clavel et al. (2000) showed that the equivalent widths of  $7.7 \mu\text{m}$  PAH emission measured with *ISO* using a large aperture ( $24 \times 24 \text{ arcsec}^2$ ) are  $\sim 8$  times larger in Seyfert 2s than in Seyfert 1s. If the  $7.7 \mu\text{m}$  PAH emission luminosities, mostly originating from extended starbursts in the host galaxies, are intrinsically the same in Seyfert 1s and 2s, then the larger equivalent widths in Seyfert 2s can be explained by the attenuation of the  $7\text{--}8 \mu\text{m}$  continuum flux from the AGN. Adopting the dust extinction curve with  $A_{7\text{--}8\mu\text{m}}/A_V \sim 0.04\text{--}0.05$  derived by Lutz et al. (1996), the dust extinction toward  $7\text{--}8 \mu\text{m}$  continuum-emission regions in Seyfert 2s is estimated to be  $A_V = 45\text{--}55$  mag. In fact, the extended PAH emission luminosities in Seyfert 2s are likely to be intrinsically larger than in Seyfert 1s (Maiolino et al. 1995), so that the above dust extinction is probably an overestimate. Although the dust extinction toward the innermost  $3\text{--}4 \mu\text{m}$  continuum-emitting region around an AGN should be larger than that toward the outer  $7\text{--}8 \mu\text{m}$  continuum-emitting region, we find no significant difference.

If the Galactic  $N_{\text{H}}/A_V$  ratio is assumed ( $\sim 2 \times 10^{21} \text{ cm}^{-2} \text{ mag}^{-1}$ ; Predehl & Schmitt 1995), dust extinction of  $A_V < 50\text{--}60$  mag implies a hydrogen column density of  $N_{\text{H}} < 10^{23} \text{ cm}^{-2}$  in the majority of Seyfert 2 nuclei, which is substantially smaller than measured values of  $N_{\text{H}}$  by X-rays toward AGNs in Seyfert 2 nuclei (Risaliti, Maiolino, & Salvati 1999; Bassani et al. 1999). Imaging observations have indicated substantially larger ratios of  $N_{\text{H}}$  (columns of X-ray absorbing material)-to- $A_V$  (dust columns toward the innermost  $3.5 \mu\text{m}$  continuum emitting regions) in Seyfert 2s (Alonso-Herrero et al. 1997, 2001, 2003). Our  $2.8\text{--}4.1 \mu\text{m}$  spectroscopy provided additional support for this.

### 5.3. Do More Powerful AGNs Have More Powerful Compact Nuclear Starbursts?

Tran (2001, 2003) argued that there are two distinct types of Seyfert 2 nuclei: one AGN-powered and another powered by a compact nuclear starburst. However, Gu & Huang (2002) did not find evidence for such distinct Seyfert 2 populations. The  $L_{3.3\text{PAH}}$  values measured from our slit spectra (Table 3) are a good measure of the absolute magnitude of the compact nuclear starbursts (Imanishi 2002), and *IRAS*  $12 \mu\text{m}$  and  $25 \mu\text{m}$  fluxes are often taken to be representative of the AGN power in a Seyfert 2 galaxy (Spinoglio & Malkan 1989; Gonzalez Delgado et al. 2001; Rodriguez Espinosa & Perez Garcia 1997). Ground-based *N*-band ( $10.6 \mu\text{m}$ ) aperture photometry of Seyfert 2 nuclei using a single-element bolometer can also be a

good tracer of AGN power (Alonso-Herrero et al. 2002) as the contamination from extended starbursts is reduced.

In Figure 2, we compare  $L_{3.3\text{PAH}}$  with *IRAS* 12- and 25- $\mu\text{m}$ , and nuclear *N*-band fluxes (Table 1). Using the generalized Kendall’s rank correlation statistic (Isobe, Feigelson, & Nelson 1986)<sup>5</sup> we found the probability that a correlation is not present to be 0.007, 0.002, and 0.001 for Fig. 2a, 2b, and 2c, respectively. Thus, we suggest that the luminosities of AGNs and compact nuclear starbursts are correlated in Seyfert 2 galaxies, so that more powerful AGNs tend to possess more powerful compact nuclear starbursts in the torus.

It has been predicted that such compact nuclear starbursts in the dusty torus can increase the mass accretion rate onto the central supermassive black hole through enhancement of the turbulence of molecular gas in the torus (von Linden et al. 1993; Wada & Norman 2002) and/or through radiation effects (Umemura, Fukue, & Mineshige 1997, 1998; Ohsuga et al. 1999). The luminosity correlation between AGNs and compact nuclear starbursts is at least in qualitative agreement with these theoretical predictions.

However, extended star formation, including circumnuclear ring-shaped starbursts and quiescent star formation in the host galaxies, may contribute to the *IRAS* 12  $\mu\text{m}$  and 25  $\mu\text{m}$  fluxes as well as to measurements from previous ground-based *N*-band photometry taken with a single element bolometer with  $> 3$  arcsec apertures. *N*-band photometry of spatially-unresolved emission using recently available two-dimensional large-format mid-infrared arrays at large telescopes (Krabbe et al. 2001) is undoubtedly a more reliable AGN indicator. These photometric data, if available for our sample in the future, could be used to investigate the connection between AGNs and compact nuclear starbursts in much greater detail.

#### 5.4. The Luminosity of Compact Nuclear Starbursts and the Covering Factor of the Dusty Torus

A compact nuclear starburst can input energy into the torus and inflate it (Fabian et al. 1998). As such an inflated torus has a large covering factor of gas and dust around the central AGN, the equivalent width of the Fe  $K\alpha$  emission line at 6.4 keV in X-rays ( $EW_{\text{Fe}}$ ) can be large. The dependence of  $EW_{\text{Fe}}$  on the covering factor at various  $N_{\text{H}}$  has been calculated by several authors (Awaki et al. 1991; Ghisellini, Haardt, & Matt 1994; Levenson et al. 2002). Both  $N_{\text{H}}$  and  $EW_{\text{Fe}}$  based on *ASCA* data are available for several sources in our sample (Bassani et al. 1999).

---

<sup>5</sup>software is available at: <http://www.astro.psu.edu/statcodes/>.

Levenson et al. (2002) performed this calculation for the Compton-thick case ( $N_{\text{H}} > 1 \times 10^{24} \text{ cm}^{-2}$ ). Four sources in our sample, NGC 7674, NGC 1667, NGC 4968, and NGC 5135, are classified as Compton thick and the  $\text{EW}_{\text{Fe}}$ s in NGC 7674, NGC 1667, NGC 4968, and NGC 5135 are estimated to be 0.9, <3, 1.18, and 11.7 keV, respectively (Bassani et al. 1999). All but NGC 1667 show a detectable compact nuclear starburst in the torus. The covering factor of the torus for NGC 7674, NGC 4968, and NGC 5135 is expected to be  $>40^\circ$  and could be as large as  $>70^\circ$  if  $N_{\text{H}}$  is close to  $1 \times 10^{24} \text{ cm}^{-2}$  (Fig. 3 of Levenson et al. 2002). However, the upper limit for  $\text{EW}_{\text{Fe}}$  in NGC 1667, the source with an undetectable compact nuclear starburst, is so large (<3 keV) that we are unable to draw meaningful conclusions about the dependence of the covering factor on the presence or absence of a compact nuclear starburst from these four sources.

In addition, Ghisellini, Haardt, & Matt (1994) performed the same calculation for the Compton-thin case ( $N_{\text{H}} < 1 \times 10^{24} \text{ cm}^{-2}$ ). For the five Compton-thin sources, NGC 4388, NGC 5252, NGC 5674, NGC 262, NGC 7172, both  $N_{\text{H}}$  and  $\text{EW}_{\text{Fe}}$  are available (Bassani et al. 1999). Compact nuclear starbursts are undetected in all of these sources, but the covering factor is expected to be  $>60^\circ$  (Fig. 3 of Ghisellini et al. 1994).

With the datasets currently available, no meaningful constraints can be obtained for the dependence of the torus covering factor on the presence of a compact nuclear starburst. However, if more accurate values of  $N_{\text{H}}$  and  $\text{EW}_{\text{Fe}}$  based on observations with *Chandra* and *XMM* (and *ASTRO-E2* for Compton-thick sources) become available for a significant number of our sample objects in the near future, then the dependence can be investigated in much more detail and the hypothesis that the compact nuclear starburst is the primary cause of inflation of the dusty molecular torus can be tested.

## 6. Summary

We have presented infrared 2.8–4.1  $\mu\text{m}$  slit spectra of 32 Seyfert 2 galaxies in the CfA and 12 $\mu\text{m}$  samples, and made the following main conclusions.

1. By using the 3.3  $\mu\text{m}$  PAH emission luminosity as an indicator of a compact nuclear starburst in the dusty torus, we found evidence for the presence of such starbursts in  $\sim 30\%$  of Seyfert 2s. However, the starbursts generally do not contribute significantly to either the observed 3–4  $\mu\text{m}$  nuclear flux or the total infrared luminosity of the observed Seyfert 2 galaxies.
2. The dust extinction in the direction of AGN-powered 3–4  $\mu\text{m}$ -continuum-emitting hot dust in the very inner part of the dusty torus, close to the dust sublimation radius, is

modest ( $A_V < 50\text{--}60$  mag) in the majority of the observed Seyfert 2 galaxies.

3. Provided that the *IRAS* 12- and 25- $\mu\text{m}$ , and nuclear *N*-band luminosities are a good measure of AGN power, the AGN and compact-nuclear-starburst luminosities are correlated.

These conclusions confirm those drawn from a smaller sample of Seyfert 2s by Imanishi (2002).

We are grateful to Dr. J. Rayner, Dr. H. Terada, Dr. S. Bus, P. Sears, W. Golisch, B. Potter, D. Scarla, and S. Harasawa for their supports during our IRTF SpeX and Subaru IRCS observing runs, and to Drs. K. Aoki, K. Wada, Y. Taniguchi, and M. Elitzur for useful discussions. This research has made use of the SIMBAD database, operated at CDS, Strasbourg, France, and of the NASA/IPAC Extragalactic Database (NED) which is operated by the Jet Propulsion Laboratory, California Institute of Technology, under contract with the National Aeronautics and Space Administration.

## REFERENCES

- Alonso-Herrero, A., Ward, M. J., & Kotilainen, J. K. 1997, *MNRAS*, 288, 977
- Alonso-Herrero, A., Simpson, C., Ward, M. J., & Wilson, A. S. 1998, *ApJ*, 495, 196
- Alonso-Herrero, A., Quillen, A. C., Simpson, C., Efstathiou, A. & Ward, M. J. 2001, *AJ*, 121, 1369
- Alonso-Herrero, A., Ivanov, V. D., Jayawardhana, R., & Hosokawa, T. 2002, *ApJ*, 571, L1
- Alonso-Herrero, A., Quillen, A. C., Rieke, G. H., Ivanov, V., & Efstathiou, A. 2003, *AJ*, 126, 81
- Antonucci, R. 1993, *ARA&A*, 31, 473
- Awaki, H., Koyama, K., Inoue, H., & Halpern, J. P. 1991, *PASJ*, 43, 195
- Barvainis, R. 1987, *ApJ*, 320, 537
- Bassani, L., Dadina, M., Maiolino, R., Salvati, M., Risaliti, G., Della Ceca, R., Matt, G., & Zamorani, G. 1999, *ApJS*, 121, 473
- Carico, D. P., Sanders, D. B., Soifer, B. T., Elias, J. H., Matthews, K., & Neugebauer, G. 1988, *AJ*, 95, 356
- Cid Fernandes, R. Jr., & Terlevich, R. 1995, *MNRAS*, 272, 423
- Cid Fernandes, R., Heckman, T., Schmitt, H., Gonzalez Delgado, R. M., & Storchi-Bergmann, T. 2001, *ApJ*, 558, 81
- Clavel, J., et al. 2000, *A&A*, 357, 839
- Devereux, N. A., Becklin, E. E., & Scoville, N. 1987, *ApJ*, 312, 529
- Dopita, M. A., Heisler, C., Lumsden, S., & Bailey, J. 1998, *ApJ*, 498, 570
- Edelson, R. A., Malkan, M. A., & Rieke, G. H. 1987, *ApJ*, 321, 233
- Efstathiou, A., & Rowan-Robinson, M. 1995, *MNRAS*, 273, 649
- Fabian, A. C., Barcons, X., Almaini, O., & Iwasawa, K. 1998, *MNRAS*, 297, L11
- Fadda, D., Giuricin, G., Granato, G. L., & Vecchies, D. 1998, *ApJ*, 496, 117
- Ghisellini, G., Haardt, F., & Matt, G. 1994, *MNRAS*, 267, 743

- Gonzalez Delgado, R. M., Heckman, T., Leitherer, C., Meurer, G., Krolik, J., Wilson, A. S., Kinney, A., & Koratkar, A. 1998, *ApJ*, 505, 174
- Gonzalez Delgado, R. M., Heckman, T., & Leitherer, C. 2001, *ApJ*, 546, 845
- Granato, G. L., & Danese, L. 1994, *MNRAS*, 268, 235
- Granato, G. L., Danese, L., & Franceschini, A. 1997, *ApJ*, 486, 147
- Gu, Q., & Huang, J. 2002, *ApJ*, 579, 205
- Heckman, T. M., Gonzalez Delgado, R., Leitherer, C., Meurer, G. R., Krolik, J., Wilson, A. S., Koratkar, A., & Kinney, A. 1997, *ApJ*, 482, 114
- Hill, G. J., Becklin, E. E., & Wynn-Williams, C. G. 1988, *ApJ*, 330, 737
- Huchra, J., & Burg, R. 1992, *ApJ*, 393, 90
- Imanishi, M. 2000, *MNRAS*, 319, 331
- Imanishi, M. 2001, *AJ*, 121, 1927
- Imanishi, M. 2002, *ApJ*, 569, 44
- Imanishi, M., Sasaki, Y., Goto, M., Kobayashi, N., Nagata, T., & Jones, T. J. 1996, *AJ*, 112, 235
- Imanishi, M., & Dudley, C. C. 2000, *ApJ*, 545, 701
- Imanishi, M., Dudley, C. C., & Maloney, P. R. 2001, *ApJ*, 558, L93
- Imanishi, M., & Maloney, P. R. 2003, *ApJ*, 588, 165
- Isobe, T., Feigelson, E. D., & Nelson, P. I. 1986, *ApJ*, 306, 490
- Ivanov, V. D., Rieke, G. H., Groppi, C. E., Alonso-Herrero, A., Rieke, M. J., & Engelbracht, C. W. 2000, *ApJ*, 545, 190
- Kobayashi, N., et al. 2000, *Proc. SPIE*, 4008, 1056
- Kohno, K., Matsushita, S., Vila-Vilaro, B., Okumura, S. K., Shibatsuka, T., Okiura, M., Ishizuki, S., Kawabe, R. 2002, in *ASP Conf. Ser.* 249, *The Central kpc of Starbursts and AGN*, 672 (astro-ph/0206398)
- Krabbe, A., Böker, T., & Maiolino, R., 2001, *ApJ*, 557, 626

- Laor, A., & Draine, B. T. 1993, *ApJ*, 402, 441
- Le Floch, E., Mirabel, I. F., Laurent, O., Charmandaris, V., Gallais, P., Sauvage, M., Vigroux, L., & Cesarsky, C. 2001, *A&A*, 367, 487
- Levenson, N. A., Krolik, J. H., Zycki, P. T., Heckman, T. M., Weaver, K. A., Awaki, H., & Terashima, Y. 2002, *ApJ*, 573, L81
- Lutz, D. et al. 1996, *A&A*, 315, L269
- Lutz, D., Maiolino, R., Moorwood, A. F. M., Netzer, H., Wagner, S. J., Sturm, E., & Genzel, R. 2002, *A&A*, 396, 439
- Maiolino, R., Ruiz, M., Rieke, G. H., & Keller, L. D. 1995, *ApJ*, 446, 561
- Maiolino, R., Marconi, A., Salvati, M., Risaliti, G., Severgnini, P., Oliva, E., La Franca, F., & Vanzi, L. 2001, *A&A*, 365, 28
- Maiolino, R., Marconi, A., & Oliva, E. 2001, *A&A*, 365, 37
- Mennella, V., Munoz Caro, G. M., Ruiterkamp, R., Schutte, W. A., Greenberg, J. M., Brucato, J. R., & Colangeli, L. 2001, *A&A*, 367, 355
- Moorwood, A. F. M. 1986, *A&A*, 166, 4
- Mountain, C. M., Robertson, D. J., Lee, T. J., & Wade, R. 1990, *Proc. SPIE*, 1235, 25
- Mouri, H., Kawara, K., Taniguchi, Y., & Nishida, M. 1990, *ApJ*, 356, L39
- Murakawa, K., Tamura, M., & Nagata, T. 2000, *ApJS*, 128, 603
- Ohsuga, K., Umemura, M., Fukue, J., & Mineshige, S. 1999, *PASJ*, 51, 345
- Oliva, E., Origlia, L., Maiolino, R., & Moorwood, A. F. M. 1999, *A&A*, 350, 9
- Osterbrock, D. E., & Martel, A. 1993, *ApJ*, 414, 552
- Pendleton, Y. J., Sandford, S. A., Allamandola, L. J., Tielens, A. G. G. M., & Sellgren, K. 1994, *ApJ*, 437, 683
- Perez Garcia, A. M., & Rogriguez Espinosa, J. M. 2001, *ApJ*, 557, 39
- Pogge, R. W., & Martini, P. 2002, *ApJ*, 569, 624
- Predehl, P., & Schmitt, J. H. M. M. 1995, *A&A*, 293, 889

- Rawlings, M. G., Adamson, A. J., & Whittet, D. C. B. 2003, *MNRAS*, 341, 1121
- Rayner, J. T., Toomey, D. W., Onaka, P. M., Denault, A. J., Stahlberger, W. E., Vacca, W. D., Cushing, M. C., & Wang, S. 2003, *PASP*, 115, 362
- Rieke, G. H. 1978, *ApJ*, 226, 550
- Risaliti, G., Maiolino, R., & Salvati, M. 1999, *ApJ*, 522, 157
- Rodriguez-Ardila, A., & Viegas, S. M. 2003, *MNRAS*, 340, L33
- Rodriguez Espinosa, J. M., & Perez Garcia, A. M. 1997, *ApJ*, 487, L33
- Rowan-Robinson, M. 1995, *MNRAS*, 272, 737
- Rush, B., Malkan, M. A., & Spinoglio, L. 1993, *ApJS*, 89, 1
- Sanders, D. B., & Mirabel, I. F. 1996, *ARA&A*, 34, 749
- Shure, M. A., Toomey, D. W., Rayner, J. T., Onaka, P., & Denault, A. J. 1994, *Proc. SPIE*, 2198, 614
- Smith, R. G., Sellgren, K., & Tokunaga, A. T. 1989, *ApJ*, 344, 413
- Smith, R. G., Sellgren, K., & Brooke, T. Y. 1993, *MNRAS*, 263, 749
- Spinoglio, L., & Malkan, M. A. 1989, *ApJ*, 342, 83
- Storchi-Bergmann, T., Wilson, A. S., & Baldwin, J. A. 1996, *ApJ*, 460, 252
- Storchi-Bergmann, T., Rodriguez-Ardila, A., Schmitt, H. R., Wilson, A. S., & Baldwin, J. A. 1996, *ApJ*, 472, 83
- Storchi-Bergmann, T., Raimann, D., Bica, E. L. D., & Fraquelli, H. A. 2000, *ApJ*, 544, 747
- Tanaka, M., Sato, S., Nagata, T., & Yamamoto, T. 1990, *ApJ*, 352, 724
- Taniguchi, Y., & Murayama, T. 1998, *ApJ*, 501, L25
- Tokunaga, A. T. 2000, in *Allen's Astrophysical Quantities*, ed. A. N. Cox (4th ed; Berlin: Springer), 143
- Toomre, A., 1964, *ApJ*, 139, 1217
- Tran, H. D. 2001, *ApJ*, 554, L19

Tran, H. D. 2003, *ApJ*, 583, 632

Umemura, M., Fukue, J., & Mineshige, S. 1997, *ApJ*, 479, L97

Umemura, M., Fukue, J., & Mineshige, S. 1998, *MNRAS*, 299, 1123

Voit, G. M. 1992, *MNRAS*, 258, 841

von Linden, S., Biermann, P. L., Duschl, W. J., Lesch, H., & Schmutzler, T. 1993, *A&A*, 280, 468

Wada, K., & Norman, C. A. 2002, *ApJ*, 566, L21

Whittet, D. C. B., Bode, M. F., Longmore, A. J., Adamson, A. J., McFadzean, A. D., Aitken, D. K., & Roche, P. F. 1988, *MNRAS*, 233, 321

Table 1. Infrared Properties of the Observed Seyfert 2 Nuclei.

Object	Redshift	$f_N$	$f_{12}$	$f_{25}$	$f_{60}$	$f_{100}$	$\log L_{\text{IR}}$	Remarks
(1)	(2)	[Jy] (3)	[Jy] (4)	[Jy] (5)	[Jy] (6)	[Jy] (7)	[ergs s <sup>-1</sup> ] (8)	(9)
Mrk 334	0.022	0.16 <sup>a</sup>	0.23	1.05	4.35	4.32	44.6	CfA
Mrk 993	0.015	0.018 <sup>b</sup>	<0.13	<0.13	0.30	1.32	43.2–43.6	CfA
Mrk 573	0.017	0.17 <sup>b</sup>	<0.25	<0.93	1.09	1.26	43.6–44.1	CfA
NGC 1144	0.029	<0.035 <sup>c</sup>	0.28	0.63	5.30	11.3	45.0	CfA, 12 $\mu$ m
NGC 4388	0.008	0.40 <sup>d</sup>	1.00	3.46	10.2	18.1	44.2	CfA, 12 $\mu$ m
NGC 5252	0.023	0.028 <sup>a</sup>	0.08 <sup>A</sup>	0.14 <sup>A</sup>	1.85 <sup>A</sup>	1.13 <sup>A</sup>	44.2	CfA
NGC 5256 (Mrk 266SW)	0.028	0.030 <sup>a</sup>	0.23	0.98	7.34	11.1	45.0	CfA, 12 $\mu$ m
NGC 5347	0.008	0.21 <sup>a</sup>	0.31	0.96	1.42	2.64	44.5	CfA, 12 $\mu$ m
NGC 5674	0.025	0.024 <sup>a</sup>	0.14	0.28	1.44	3.73	44.4	CfA
NGC 5695	0.014	<0.01 <sup>a</sup>	<0.11	0.13	0.57	1.79	43.4–43.6	CfA
NGC 5929	0.008	0.024 <sup>a</sup>	0.43	1.62	9.14	13.7	44.1	CfA, 12 $\mu$ m
NGC 7674	0.029	0.33 <sup>a</sup>	0.67	1.90	5.59	8.15	45.1	CfA, 12 $\mu$ m
NGC 7682	0.017	0.012 <sup>a</sup>	0.32 <sup>A</sup>	0.22 <sup>A</sup>	0.47 <sup>A</sup>	0.41 <sup>A</sup>	43.9	CfA
Mrk 938	0.019	0.24 <sup>a</sup>	0.40	2.37	16.6	17.2	45.0	12 $\mu$ m
NGC 262 (Mrk 348)	0.015	0.30 <sup>e</sup>	0.31	0.83	1.29	1.55	44.0	12 $\mu$ m
NGC 513	0.020		0.17	0.28	1.94	4.05	44.3	12 $\mu$ m
F01475–0740	0.017	0.21 <sup>f</sup>	0.31	<0.96	1.05	0.65	43.9–44.1	12 $\mu$ m
NGC 1125	0.011		0.17	0.83	3.31	3.94	43.9	12 $\mu$ m
NGC 1194	0.013		0.27	0.51	0.77	<0.93	43.7	12 $\mu$ m
NGC 1241	0.014	0.08 <sup>a</sup>	0.24	0.45	3.56	10.3	44.2	12 $\mu$ m
NGC 1320 (Mrk 607)	0.010	0.028 <sup>a</sup>	0.33	1.07	2.15	2.75	43.8	12 $\mu$ m
F04385–0828	0.015	0.27 <sup>a</sup>	0.42	1.62	2.77	2.53	44.3	12 $\mu$ m
NGC 1667	0.015	0.005 <sup>a</sup>	0.43	0.68	5.95	14.7	44.5	12 $\mu$ m
NGC 3660	0.012	0.033 <sup>a</sup>	0.19	0.22	1.87	4.54	43.8	12 $\mu$ m
NGC 4501	0.008	0.006 <sup>a</sup>	1.02	1.28	13.7	54.7	44.4	12 $\mu$ m
NGC 4968	0.010	0.12 <sup>a</sup>	0.39	1.05	2.38	2.94	43.8	12 $\mu$ m
MCG-3-34-64	0.017	0.44 <sup>a</sup>	0.88	2.86	5.90	5.48	44.7	12 $\mu$ m
NGC 5135	0.014	0.16 <sup>a</sup>	0.64	2.40	16.9	28.6	44.8	12 $\mu$ m
MCG-2-40-4	0.024		0.39	0.86	3.65	6.53	44.7	12 $\mu$ m
F15480–0344	0.030		0.18	0.73	1.07	<4.05	44.5–44.6	12 $\mu$ m
NGC 7172	0.009		0.44	0.76	5.71	12.3	44.0	12 $\mu$ m
MCG-3-58-7	0.032		0.28	0.80	2.42	3.36	44.8	12 $\mu$ m

Note. — Column (1): Object. CfA Seyfert 2s are placed first. Ordered by right ascension in each Seyfert 2 sample. Column (2): Redshift. Column (3): Ground-based  $N$ -band (10.6  $\mu$ m) photometry and references. (a): Maiolino et al. (1995), (b): Edelson, Malkan, & Rieke (1987), (c): Carico et al. (1988), (d): Devereux, Becklin, & Scoville (1987), (e): Rieke (1978), (f): Hill, Becklin, & Wynn-Williams (1988). Columns (4)–(7):  $f_{12}$ ,  $f_{25}$ ,  $f_{60}$ , and  $f_{100}$  are *IRAS FSC* fluxes at 12 $\mu$ m, 25 $\mu$ m, 60 $\mu$ m, and 100 $\mu$ m, respectively. Column (8): Logarithm of infrared (8–1000  $\mu$ m) luminosity in ergs s<sup>-1</sup> calculated with  $L_{\text{IR}} = 2.1 \times 10^{39} \times D(\text{Mpc})^2 \times (13.48 \times f_{12} + 5.16 \times f_{25} + 2.58 \times f_{60} + f_{100})$  ergs s<sup>-1</sup> (Sanders & Mirabel 1996). Column (9): CfA (Huchra & Burg 1992) or 12  $\mu$ m (Rush et al. 1993) Seyfert 2s.

<sup>A</sup>ISO measurements (Perez Garcia & Rodriguez Espinosa 2001). The  $f_{12}$  and  $f_{100}$  are extrapolated and interpolated, respectively, from measurements at other wavelengths.

Table 2. Observing Log.

Object	Date (UT)	Telescope & Instrument	Integration Time (min)	Standard Star			
				Star Name	<i>L</i> -mag	Type	$T_{\text{eff}}$ (K)
Mrk 334	2002 Aug 19	Subaru IRCS	20	HR 8955	5.1	F6V	6400
Mrk 993	2002 Aug 27, 29	IRTF SpeX	100	HR 410	5.0	F7V	6240
Mrk 573	2002 Aug 28	IRTF SpeX	30	HR 650	4.1	F8V	6000
NGC 1144	2002 Oct 24	Subaru IRCS	16	HR 962	3.7	F8V	6000
NGC 4388	2003 Mar 18	IRTF SpeX	30	HR 4708	5.0	F8V	6000
NGC 5252	2003 Mar 19	IRTF SpeX	40	HR 5011	3.8	G0V	5930
NGC 5256	2001 Apr 9	IRTF NSFCAM	36	HR 4767	4.8	F8V–G0V	6000
NGC 5347	2003 Mar 18	IRTF SpeX	40	HR 5346	4.8	F8V	6000
NGC 5674	2002 Mar 28	Subaru IRCS	12	HR 5386	5.1	A0V	9480
NGC 5695	2003 Mar 20	IRTF SpeX	60	HR 5630	4.9	F8V	6000
NGC 5929	2002 Aug 29	IRTF SpeX <sup>a</sup>	40	HR 5728	4.5	G3V	5800
NGC 7674	2002 Aug 27	IRTF SpeX	20	HR 8653	4.6	G8IV	5400
NGC 7682	2002 Aug 27, 29	IRTF SpeX	160	HR 8969	2.8	F7V	6240
Mrk 938	2002 Aug 28	IRTF SpeX	30	HR 8917 <sup>b</sup>	4.9	G0V	5930
NGC 262	2002 Aug 28	IRTF SpeX	30	HR 410	5.0	F7V	6240
NGC 513	2002 Aug 28	IRTF SpeX	30	HR 410	5.0	F7V	6240
F01475–0740	2002 Aug 27	IRTF SpeX	30	HR 466	4.9	F7V	6240
NGC 1125	2002 Oct 24	Subaru IRCS	8	HR 784	4.5	F6V	6400
NGC 1194	2002 Aug 28	IRTF SpeX	30	HR 996	3.2	G5V	5700
NGC 1241	2002 Aug 29	IRTF SpeX	50	HR 784	4.5	F6V	6400
NGC 1320	2002 Aug 29	IRTF SpeX	30	HR 784	4.5	F6V	6400
F04385–0828	2002 Aug 29	IRTF SpeX	30	HR 1536	4.4	F8V	6000
NGC 1667	2003 Mar 20	IRTF SpeX	60	HR 1536	4.4	F8V	6000
NGC 3660	2003 Mar 20	IRTF SpeX	90	HR 4529	4.9	F7V	6240
NGC 4501	2003 Mar 18	IRTF SpeX	40	HR 4708	5.0	F8V	6000
NGC 4968	2003 Mar 20	IRTF SpeX	30	HR 4935	4.2	F7V	6240
MCG-3-34-64	2003 Mar 19	IRTF SpeX	40	HR 4995	3.6	G6V	5620
NGC 5135	2001 Apr 8	IRTF NSFCAM	36	HR 5212	4.8	F7V	6240
MCG-2-40-4	2003 Mar 19	IRTF SpeX	40	HR 5779	5.2	F7V	6240
F15480–0344	2002 Aug 29	IRTF SpeX	30	HR 5779	5.2	F7V	6240
NGC 7172	1999 Sep 9	UKIRT CGS4	53.3	HR 8087	5.3	A0V	9480
MCG-3-58-7	2002 Aug 28	IRTF SpeX	20	HR 8457	4.8	F6V	6400

<sup>a</sup>3–4  $\mu\text{m}$  spectrum taken with IRTF NSFCAM was presented in Imanishi (2002), but the presence of the 3.3  $\mu\text{m}$  PAH emission was unclear. This source was re-observed using IRTF SpeX.

<sup>b</sup>Flux calibration was made using HR 8457.

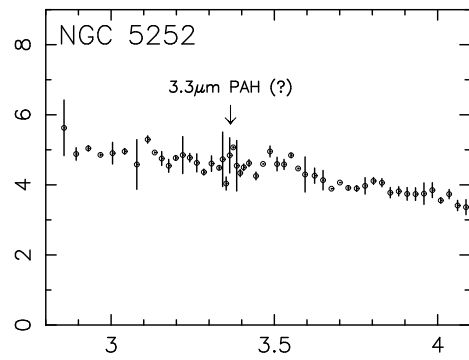
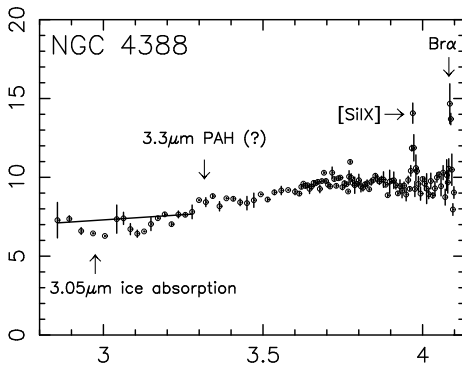
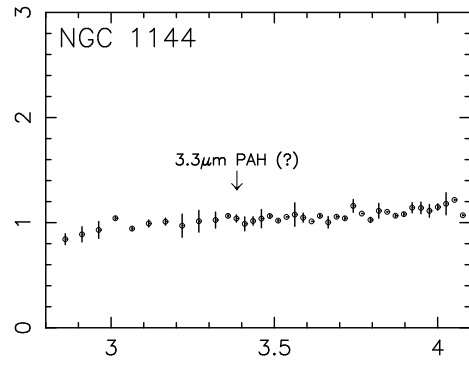
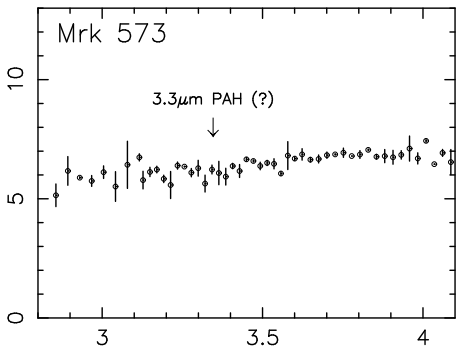
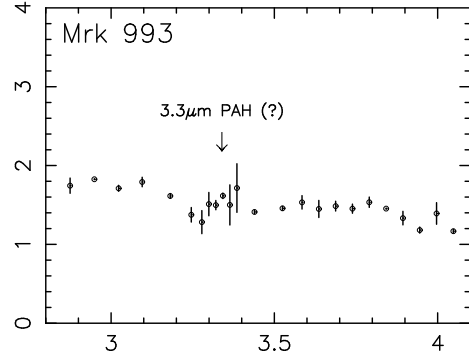
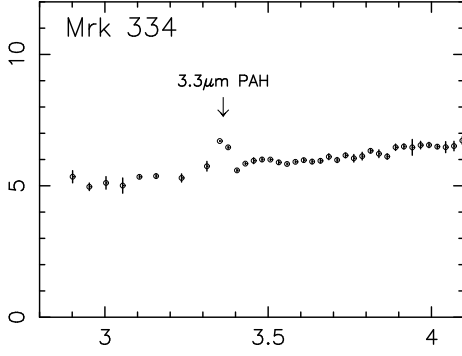
Table 3. The Properties of the 3.3  $\mu\text{m}$  PAH Emission Feature.

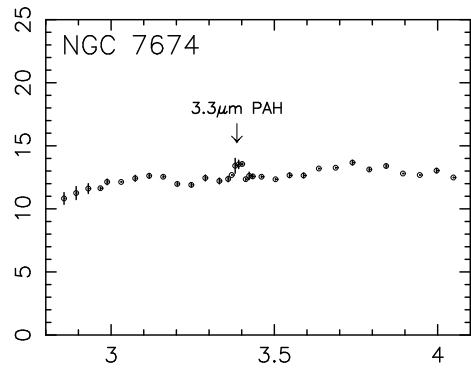
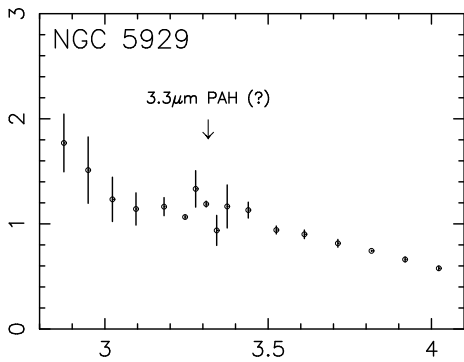
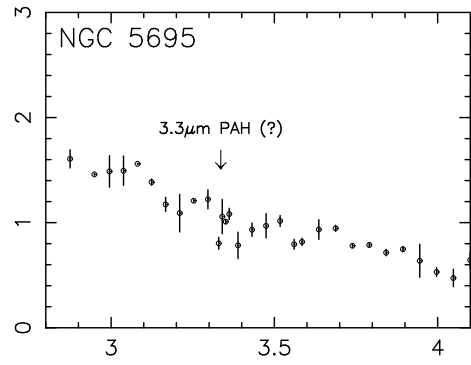
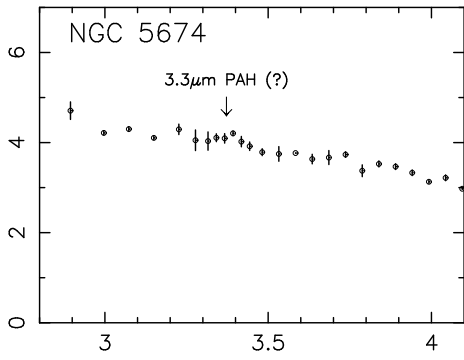
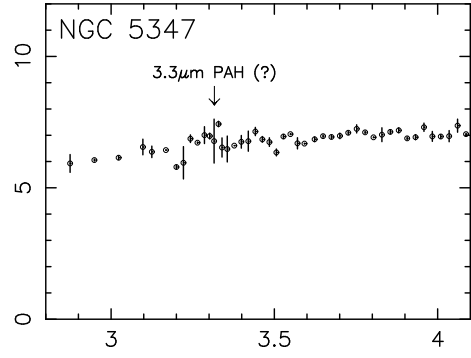
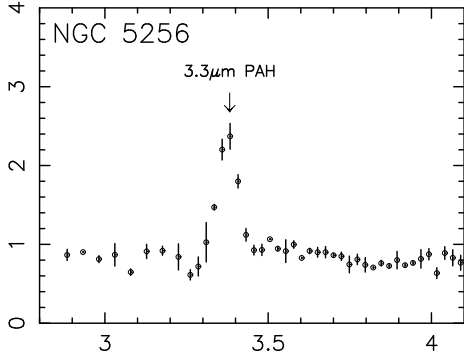
Object (1)	$f_{3.3\text{PAH}}$ ( $\times 10^{-14}$ ergs s $^{-1}$ cm $^{-2}$ ) (2)	$L_{3.3\text{PAH}}$ ( $\times 10^{39}$ ergs s $^{-1}$ ) (3)	$L_{3.3\text{PAH}}/L_{\text{IR}}$ ( $\times 10^{-3}$ ) (4)	rest EW $_{3.3\text{PAH}}$ (nm) (5)
Mrk 334	6.1 $\pm$ 0.1	58 $\pm$ 1	0.1	11
Mrk 993	<2.2	<9.4	<0.6	<16
Mrk 573	<3.2	<18	<0.5	<6
NGC 1144	<0.7	<12	<0.02	<7
NGC 4388	<3.8	<4.7	<0.03	<5
NGC 5252	<5.4	<56.4	<0.4	<12
NGC 5256	8.5 $\pm$ 0.5	133 $\pm$ 7	0.1 <sup>a</sup>	87
NGC 5347	<6.4	<7.9	<0.3	<10
NGC 5674	<1.5	<19	<0.08	<4
NGC 5695	<1.6	<6.1	<0.3	<16
NGC 5929	<1.4	<1.7	<0.02	<13
NGC 7674	8.1 $\pm$ 0.5	136 $\pm$ 8	0.1	7
NGC 7682	2.0 $\pm$ 0.5	11 $\pm$ 3	0.2	40
Mrk 938	41 $\pm$ 1	289 $\pm$ 3	0.3	75
NGC 262	<8.6	<38	<0.4	<7
NGC 513	<2.7	<22	<0.2	<6
F01475-0740	3.9 $\pm$ 0.5	22 $\pm$ 3	0.3	21
NGC 1125	10.2 $\pm$ 1.4	24 $\pm$ 3	0.3	50
NGC 1194	<2.7	<8.8	<0.2	<4
NGC 1241	<1.1	<4.1	<0.03	<12
NGC 1320	<5.9	<12	<0.2	<8
F04385-0828	4.1 $\pm$ 0.3	18 $\pm$ 1	0.1	4
NGC 1667	<1.6	<7.1	<0.03	<16
NGC 3660	4.0 $\pm$ 1.1	11 $\pm$ 3	0.2	50
NGC 4501	<3.8	<4.7	<0.02	<12
NGC 4968	8.5 $\pm$ 1.1	17 $\pm$ 2	0.2	18
MCG-3-34-64	<3.3	<18	<0.04	<6
NGC 5135	15 $\pm$ 3	58 $\pm$ 11	0.09	24
MCG-2-40-4	<7.1	<80	<0.2	<3
F15480-0344	<3.3	<59	<0.2	<11
NGC 7172	<5.3 <sup>b</sup>	<8.4 <sup>b</sup>	<0.08 <sup>b</sup>	<3.5 <sup>b</sup>
MCG-3-58-7	<3.8	<78	<0.2	<3

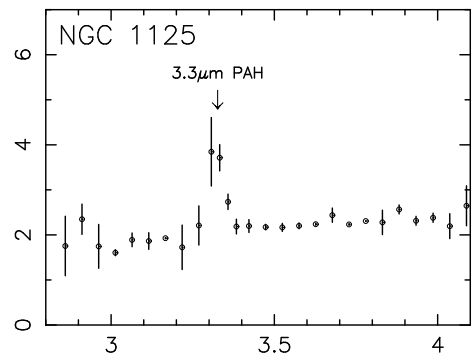
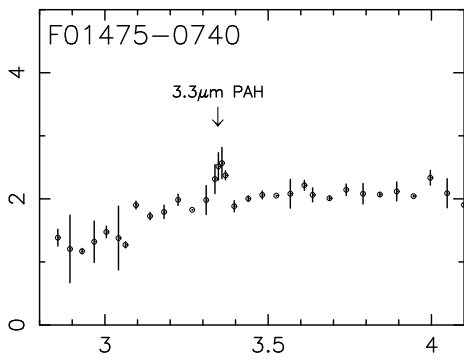
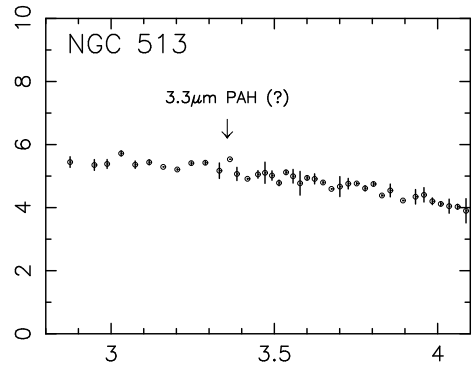
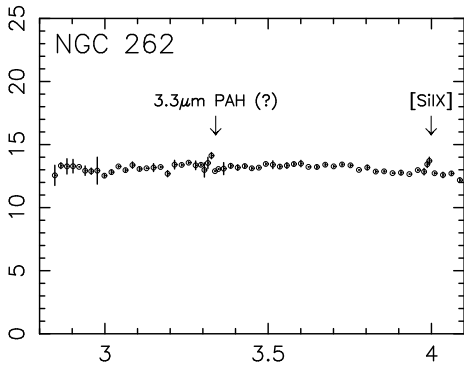
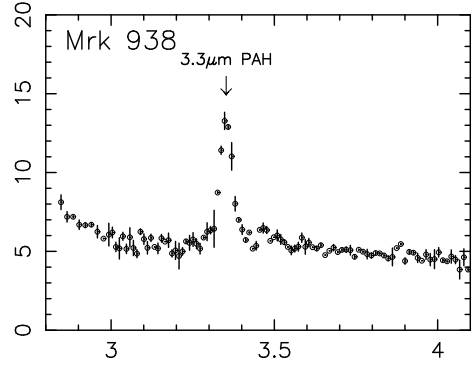
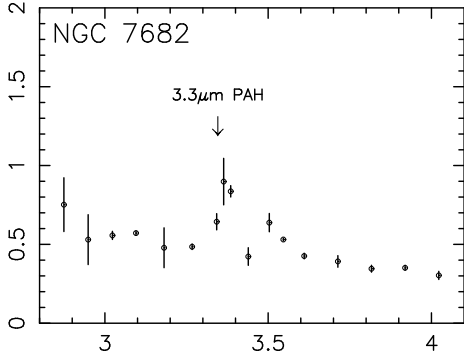
Note. — Column (1): Object. Column (2): Observed 3.3  $\mu\text{m}$  PAH flux. Column (3): Observed 3.3  $\mu\text{m}$  PAH luminosity. Column (4): Observed 3.3  $\mu\text{m}$  PAH to infrared luminosity ratio in units of  $10^{-3}$ , the typical value for starburst galaxies. Column (5): Rest frame equivalent width of the 3.3  $\mu\text{m}$  PAH emission.

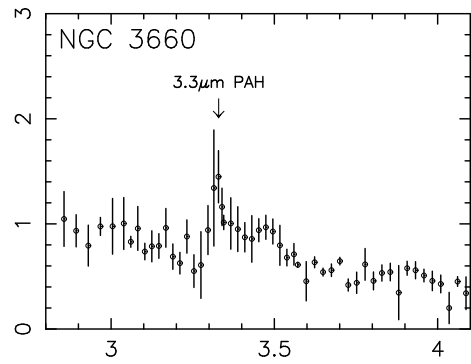
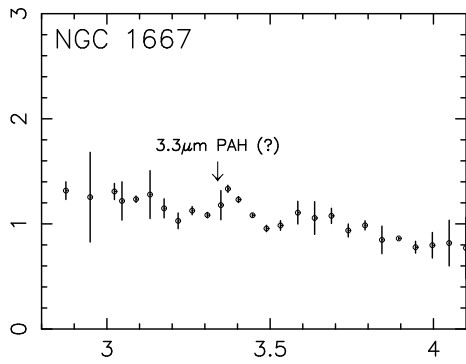
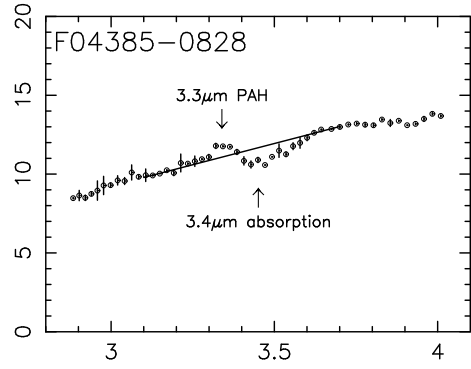
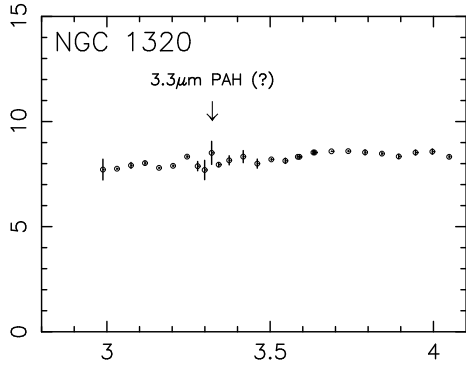
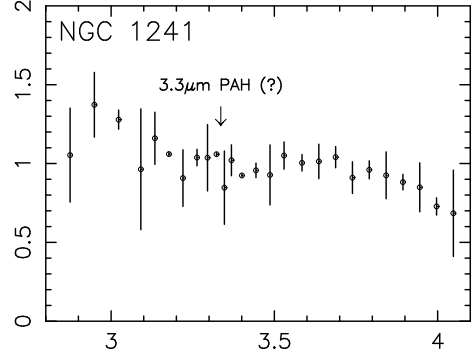
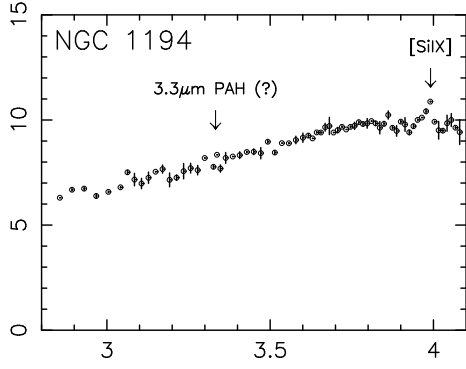
<sup>a</sup>NGC 5256 is a double-nuclei source. The  $L_{3.3\text{PAH}}$  is for only one nucleus (Mrk 266 SW), whereas both nuclei contribute to  $L_{\text{IR}}$ .

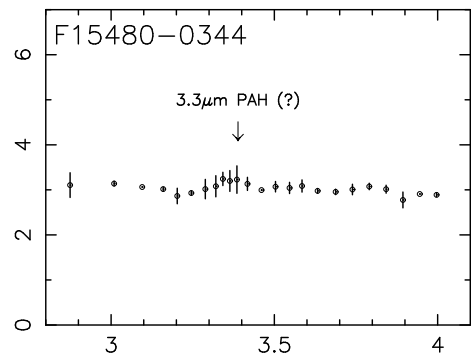
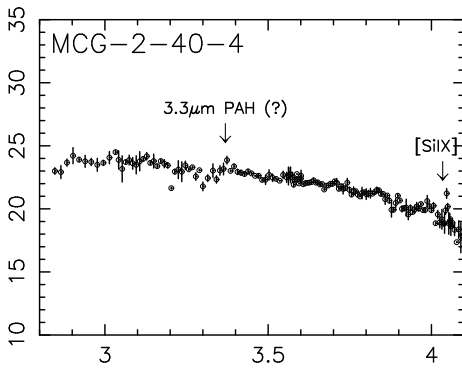
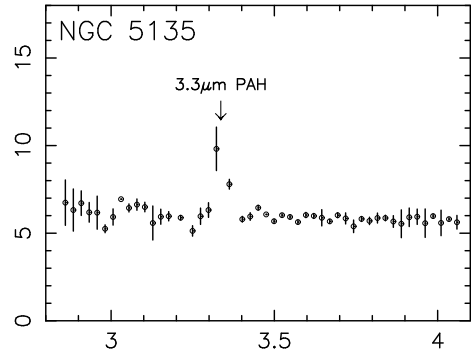
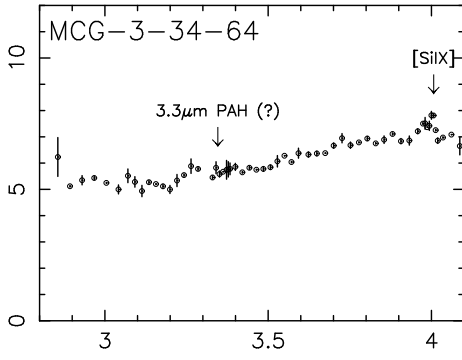
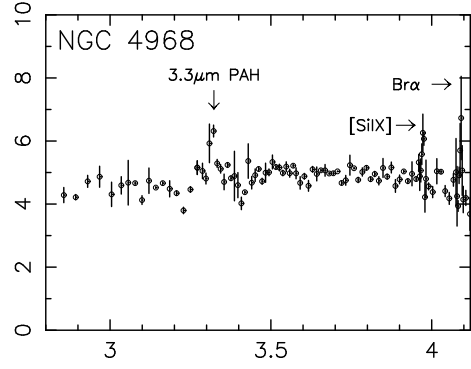
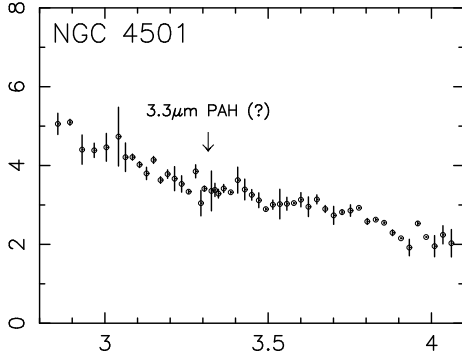
<sup>b</sup>An upper limit was re-calculated after Imanishi (2000).











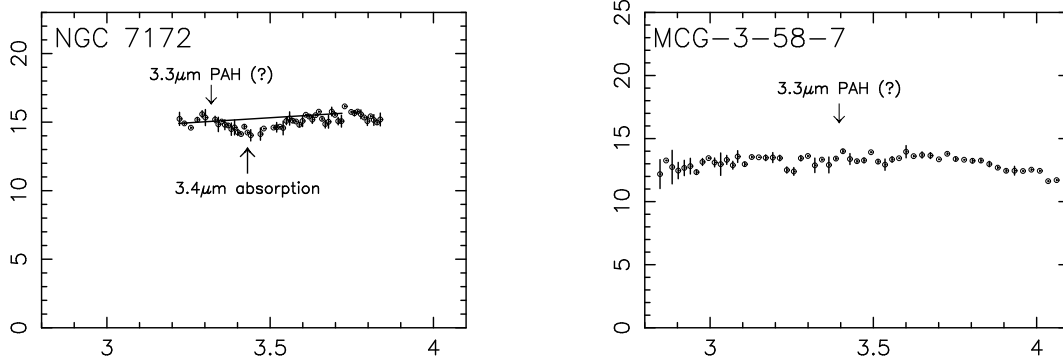


Fig. 1.— Infrared 2.8–4.1  $\mu\text{m}$  spectra of the 32 Seyfert 2 nuclei. The abscissa and ordinate are the observed wavelength in  $\mu\text{m}$  and  $F_\lambda$  in  $10^{-15} \text{ W m}^{-2} \mu\text{m}^{-1}$ , respectively. For NGC 4388, F04385–0828, and NGC 7172, the solid lines are the adopted continuum levels, with respect to which the optical depths of the absorption feature at 3.1  $\mu\text{m}$  or 3.4  $\mu\text{m}$  were measured.

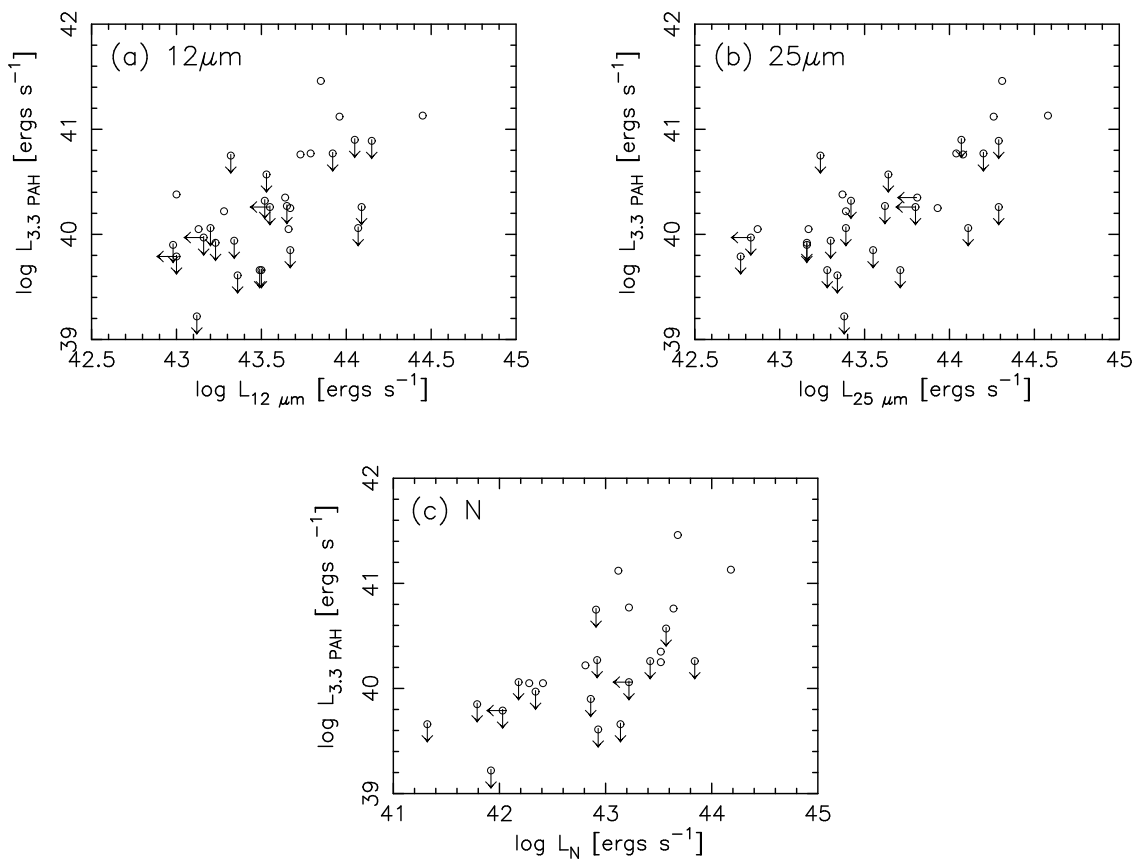


Fig. 2.— (a): The comparison of the *IRAS* 12  $\mu\text{m}$  luminosity, defined as  $\nu L_\nu$  (abscissa), and 3.3  $\mu\text{m}$  PAH emission luminosity detected inside our slit spectra (ordinate). (b): Same as (a), but the abscissa is *IRAS* 25  $\mu\text{m}$  luminosity. (c): Same as (a), but the abscissa is *N*-band (10.6  $\mu\text{m}$ ) luminosity measured with ground-based aperture photometry.